Molecular Biology of the Cell
Vol. 17, 2424–2438, May 2006

Motion Matters: Secretory Granule Motion Adjacent to the Plasma Membrane and Exocytosis

Miriam W. Allersma,*† Mary A. Bittner,* Daniel Axelrod,† and Ronald W. Holz*

*Department of Pharmacology and †Biophysics Research Division, Department of Physics, University of Michigan, Ann Arbor, MI 48109-0632

Submitted October 11, 2005; Revised February 15, 2006; Accepted February 22, 2006
Monitoring Editor: Jennifer Lippincott-Schwartz

Total internal reflection fluorescence microscopy was used to monitor changes in individual granule motions related to the secretory response in chromaffin cells. Because the motions of granules are very small (tens of nanometers), instrumental noise in the quantitation of granule motion was taken into account. ATP and Ca^{2+}, both of which prime secretion before fusion, also affect granule motion. Removal of ATP in permeabilized cells causes average granule motion to decrease. Nicotinic stimulation causes a calcium-dependent increase in average granule motion. This effect is more pronounced for granules that undergo exocytosis than for those that do not. Fusion is not preceded by a reduction in mobility. Granules sometimes move 100 nm or more up to and within a tenth of a second before fusion. Thus, the jittering motion of granules adjacent to the plasma membrane is regulated by factors that regulate secretion and may play a role in secretion. Motion continues until shortly before fusion, suggesting that interaction of granule and plasma membrane proteins is transient. Disruption of actin dynamics did not significantly alter granule motion.

INTRODUCTION

Our current notions of different granule pools and the dynamics of events immediately before fusion result in large part from inferences based upon secretion kinetics. In these experiments, granule pools are defined by the rates at which granules fuse with the plasma membrane after a Ca^{2+} stimulus and the manner in which the kinetics is altered by biochemical manipulations. A commonly held assumption is that some granules are stably bound to the plasma membrane, where they undergo priming before they are competent to undergo exocytosis.

Another view of granule behavior comes from quantitative studies of granule motion in PC12 cells (Burke *et al*., 1997; Han *et al*., 1999; Ng *et al*., 2003), neurons (Shakiryanova *et al*., 2005; Silverman *et al*., 2005), and neuroendocrine cells (Steyer *et al*., 1997; Oheim *et al*., 1998; Oheim and Stuhmer, 2000; Tsuboi *et al*., 2000; Johns *et al*., 2001; Ohara-Imaizumi *et al*., 2002; Allersma *et al*., 2004; Ivarsson *et al*., 2004) using wide field, confocal, and especially total internal reflection fluorescence microscopy (TIRFM) of fluorescently tagged secretory granules. The latter technique selectively illuminates the aqueous phase immediately adjacent to a glass interface with an exponentially decaying excitation (the evanescent field, decay constant 50–100 nm) (Axelrod, 1981, 2001, 2003; Axelrod *et al*., 1984; Stout and Axelrod, 1989). Secretory granules in these cells display a variety of different behaviors. For example, granules in growth cones of PC12 cells (Burke *et al*., 1997; Han *et al*., 1999; Ng *et al*., 2003) have slow, diffusive motions, whereas granules in growth cones and processes of hippocampal neurons have directed as well as diffusive motions (Silverman *et al*., 2005).

A common finding in TIRFM studies in chromaffin cells is that the majority of the granules adjacent to the plasma membrane are highly restricted in their motion (Steyer *et al*., 1997; Oheim *et al*., 1998; Han *et al*., 1999; Johns *et al*., 2001; Ohara-Imaizumi *et al*., 2002) as if tethered or caged. The relationship of these granules to the plasma membrane is unknown. Most of the secretory events occur from these granules. More mobile, protein-containing granules in PC12 cell (Ng *et al*., 2003) and hippocampal (Silverman *et al*., 2005) growth cones also undergo fusion, and there is evidence that enhanced mobility increases the probability of fusion (Ng *et al*., 2003).

In primary secretory cells quantitative investigations of the regulation of granule motion have been hampered by the fact that the motions are small and variable. In the present study in chromaffin cells, we overcame some of the technical difficulties and investigated granule motion adjacent to the plasma membrane under basal conditions and during the secretory response. We developed a quantitative approach to estimate and correct for noise in the measurements. To deal with the cell-to-cell and granule-to-granule variability, methods were devised to investigate the regulation of granule motion in which each cell or granule served as its own control. There were a number of important findings. ATP and Ca^{2+}, both of which prime secretion before fusion, increase granule motion. In addition, granules destined to undergo secretion show random motions to within 100–200 ms of fusion with some granules moving 200 nm or more within 100 ms of fusion.

This article was published online ahead of print in *MBC in Press* (http://www.molbiolcell.org/cgi/doi/10.1091/mbc.E05–10–0938) on March 1, 2006.

Address correspondence to: Miriam W. Allersma (allersma@umich.edu).

Abbreviations used: DMPP, 1,1 dimethyl-4-phenylpiperzinium; GFP, green fluorescent protein; NaGEP, sodium glutamate solution with EGTA and PIPES; PSS, physiological salt solution; *R* motion, motion in the plane of the coverslip (*x*,*y*); TIRFM, total internal reflection fluorescence microscopy.

© 2006 by The American Society for Cell Biology

MATERIALS AND METHODS

Chromaffin Cell Preparation and Transfection

Chromaffin cell preparation and transient transfection were performed as described previously (Wick *et al*., 1993; Holz *et al*., 1994). For TIRFM, cells were plated onto coverslips with a refractive index of 1.78. Coverslips were sequentially coated with poly-D-lysine and calf skin collagen to promote cell adhesion. Ca^{2+} phosphate precipitation (Wilson *et al*., 1996) was used for transfection. Cells where transfected with one of two plasmids: vesicle-associated membrane protein-green fluorescent protein (VAMP-GFP) or atrial natriuretic peptide (ANP)-GFP. The mammalian expression vector for VAMP2 fused on the C terminus (lumenal) to enhanced green fluorescent protein (EGFP) was a gift from Dr. Richard Scheller (Stanford University, Stanford, CA, and Genentech, South San Francisco, CA).

The ANP-emeraldGFP (ANP-GFP) was generously provided by Dr. Edwin Levitan (University of Pittsburgh, Pittsburgh, PA). ANP-GFP is directed to the regulated exocytotic pathway and packaged into secretory granules. Experiments were performed 4–8 d after transfection.

Perfusion Experiments

Intact cell stimulation experiments were performed in a physiological salt solution (PSS) containing 145 mM NaCl, 5.6 mM KCl, 2.2 mM $CaCl_2$, 0.5 mM $MgCl_2$, 15 HEPES, pH 7.4, and 5 mg/ml bovine serum albumin at ~22°C unless otherwise indicated. Individual cells were continually perfused with PSS that was continuously delivered to individual cells through a 0.2-μm inner diameter quartz pipet under positive pressure. Cells were stimulated by switching to PSS containing the nicotinic agonist 20 μM 1,1 dimethyl-4-phenylpiperzinium (DMPP) for 5–10 s. Permeabilized cell experiments were performed in a sodium glutamate solution (NaGEP) containing 139 mM sodium glutamate, 20 mM PIPES, 2 mM MgATP, and 5 mM EGTA, pH 6.6, with no added Ca^{2+}. Individual cells were continually perfused with NaGEP and then permeabilized by switching to NaGEP containing 20 μM digitonin for 30 s. Perfusion continued with NaGEP for another minute and then switched to NaGEP with or without ATP for a final minute.

Total Internal Reflection Fluorescence Microscopy

Prismless (through-the-objective) TIRFM was obtained by directing an Argon ion laser (488 line; Melles Griot [Carlsbad, CA] model 35-LAP-431-208 or 3W Lexel [Fremont, CA] model 95) through a custom side port to a side-facing dichroic mirror Q495LPw/AR (Chroma Technology) and a HQ500 LP emission filter (Chroma Technology, Brattleboro, VT) on an Olympus IX70 (inverted) microscope (Olympus, Melville, NY). The beam was focused on the periphery of the back focal plane of a 100× 1.65 numerical aperture, oil immersion objective (Olympus) so that the laser beam was incident on the coverslip at 58.4–64.2° from the normal giving a decay constant for the evanescent field of 48–62 nm. A value of 55 nm was used for calculation. Digital images were captured on a cooled charge-coupled device (CCD) camera (SensiCam QE or SensiCam; Cooke, Romulus, MI). Images were acquired at 2 Hz (permeabilization experiments) or 10–14 Hz (stimulation experiments) with exposure times of 20–50 ms. During an experiment, cells were perfused using a computer-controlled perfusion apparatus (model DAD-6VM; ALA Scientific Instruments, Westbury, NY).

Image Analysis

Granules were identified and tracked through a time-sequence stack of images using software written by the authors in Interactive Data Language (Research Systems, Boulder, CO) with methods similar to those described previously (Johns *et al*., 2001). From the stack of images, a data set was generated containing x and y coordinates, granule intensity and local background for each granule in each frame, as follows. The x and y positions were determined from band pass filtered images by solving for the peak position of a parabola that was fit to the measured intensity of the central (brightest) pixel and the immediately adjacent pixels on either side, in x and y, respectively. Total granule intensity was determined from unfiltered images by integrating pixel intensities within a circular region (600 nm in diameter; 81 pixels) around the granule center after the local background was subtracted. The local background was the average intensity of a ring of 32 pixels just outside the circle. The data set was then analyzed to track granules, calculate interframe motions, and determine other parameters as indicated in the results and in the figure legends. In the stimulation experiments, the frame just before exocytosis, f_0, was identified as the frame before the occurrence of significant increases in fluorescence intensity or width (see below).

Noise Analysis

To determine the contribution of intensity fluctuations from instrumental noise (shot noise plus CCD readout noise) to the measured granule motions, we measured the intensity and x,y position fluctuations of immobilized fluorescent particles (either 200-nm-diameter microspheres or cellular debris, possibly actual granules escaped from a damaged cell). If the instrumental noise is due in part to shot noise, then it will depend on intensity. The excitation intensity was varied 1000-fold with neutral density filters. We derived an expression to correct average motions for the noise (see Appendix) and used this method on all of the data presented. By simulating the noise of the observed characteristics with a Monte-Carlo–type program, we could also calculate the uncertainties in the final estimates for the average z and R motions as well as the probabilities that individual measurements were not purely instrumental noise. Noise corrections were generally insignificant for R motions but more significant for z motions, especially when dimmer granules are considered (Figure 1). Noise considerations impacted the data in three ways: 1) Average motions less than twice the estimated noise were excluded from analyses. When individual motions were considered, motions outside the 95% confidence intervals were excluded (e.g., ~50% of the selected granules undergoing exocytosis were excluded from z motion analysis in Figure 6, A and B). 2) Noise-corrected motions were less than uncorrected motions. 3) Noise corrections increased the standard deviations.

Analysis of the Postfusion Fluorescence

A 27- × 27-pixel (1.62- × 1.62-μm) region of interest (ROI) around the granule was chosen to accommodate the fluorescence spread that occurs after fusion. For frames f_0 and earlier, granule intensity was calculated as described above. In frame f_0, a residue intensity was defined as the total ROI intensity minus the granule intensity. For frames after f_0, the intensity of the spreading granule was calculated as the total ROI intensity minus this residue. This residue was defined as the total ROI intensity.

RESULTS

Correction of Calculated Granule Motion for Instrumental Noise

Numerous studies using TIRFM have determined that the brightest-looking chromaffin granules, those immediately adjacent to the plasma membrane, are highly restricted in their frame-to-frame motion, as if they are tethered or caged (Steyer *et al*., 1997; Oheim *et al*., 1998; Johns *et al*., 2001). Dimmer, presumably more distant, granules seem to move faster. However, it is likely that some of the reported motion may arise as an artifact of instrument noise (shot noise + CCD readout noise), which would cause apparent fluctuations in intensity or central x-y positions even on theoretically immobile objects. Noise may account for the apparent higher mobility seen in dim granules. We show in the Appendix how to correct for the noise and calculate the uncertainty in the corrected calculations for $<(\Delta z)^2>$ and $<(\Delta R)^2>$. Corrected results for these motions versus z position (relative to the plasma membrane) are shown in Figure 1. The z motion measurements uncorrected for noise overestimate z motion. Nevertheless, the changes in the actual motions with distance from the plasma membrane confirm the previous observation of greater restriction of z motion of membrane-proximal (brighter) granules. Average Δz^2 motion plateau at ~18 nm^2 or Δz = ~4 nm at an apparent z position of 30 nm. Except for the motion at the apparent z position of 4 nm, all the average z motions are significantly greater than 0 (>95% probability).

Noise contributions in measurements of R (x,y) motion are small or insignificant over the range of apparent z positions 4–200 nm. (See Appendix for a discussion of the difference in noise in the Δz and ΔR measurements.) R motions also increase with increasing apparent z positions. Average ΔR^2 was ~900 nm^2 or ΔR = ~30 nm at an apparent z position of 30 nm. Motion perpendicular to the plasma membrane (z motion) is significantly more restricted than motion parallel to the plasma membrane (R motion) at all apparent z positions. In the following quantitative analyses of granule motion, noise was taken into account and the estimated actual motions presented.

ATP and Granule Motion

ATP primes the secretory pathway before Ca^{2+} triggers fusion (Holz *et al*., 1989; Bittner and Holz, 1992; Hay and Martin, 1992). ATP can act through several mechanisms that would alter granule motion (see *Discussion*). The effect of

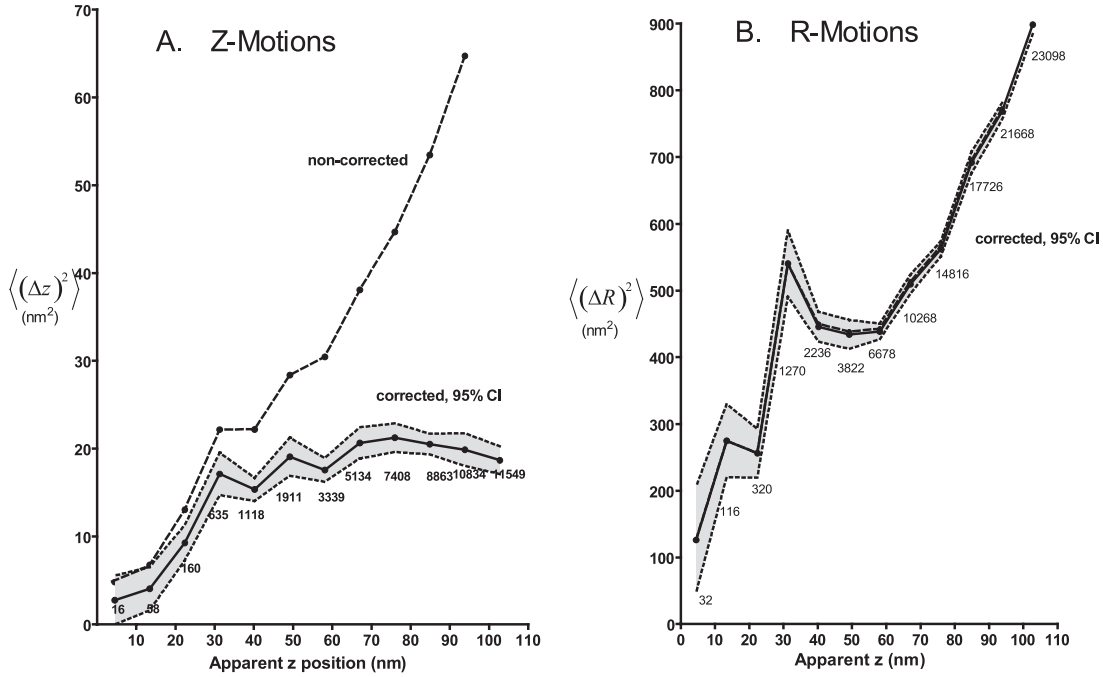

Figure 1. $<(\Delta z)^2>$ and $<(\Delta R)^2>$ versus z corrected for noise. The apparent z position is based on the observed average intensity between successive pairs of z or R measurements, with the corresponding Δz or ΔR placed in the appropriate uniformly spaced z bin. The brightest granule in the cell is used to define $z = 0$. Uncorrected values are straight averages of the $(\Delta z)^2$ or $(\Delta R)^2$ in each bin. The corrected values take into account that part of the uncorrected values that arise from instrumental noise, as described in the Appendix. The gray band around the corrected values represent the $\pm 2 \times$ SE (i.e., 95% confidence) values, as calculated according to the Appendix. The uncorrected and corrected average R motions almost overlap. With the correction and the uncertainty band, one can see that the real motion both for Δz or ΔR is significant at all apparent z positions, it increases with z, and it is generally larger for R (the lateral direction) than for z (orthogonal to the substrate and presumably the membrane).

ATP on granule motion was investigated in permeabilized cells. Individual cells were permeabilized by perfusion with solution containing digitonin (20 μM) and ATP and then perfused for 1 min with solution containing ATP (without digitonin). The perfusion was then switched to a solution with or without ATP for a final minute. Due to cell-to-cell variability, two analyses were performed in which each cell or granule served as its own control. In one analysis, changes in granule motion were quantitated from a series of difference images in which each image was subtracted, pixel by pixel, from the preceding image (Figure 2). This method detected a wide range of R motions from ~50 nm to hundreds of nanometers. Examples of difference-images from two cells are shown in Figure 2. An isolated dark spot reflects a granule moving away from the glass interface, whereas an isolated light spot reflects a granule moving toward the interface (examples indicated by black and white circles, respectively, in Figure 2A). A pair of immediately adjacent dark and light spots reflects a granule moving laterally in the evanescent field in the direction of dark to light. The R motion of a pair indicated by an adjacent the white arrow (Figure 2B) was 50 nm (measured in the original images). After ATP removal, the light and dark spots were fewer and less intense (Figure 2B). The overall degree of motion was quantitated for the entire time series of difference images. Because both negative and positive intensity differences indicate movement, pixels with an absolute value greater than a threshold were counted, N_a. Threshold values were large enough to exclude pixel differences which were in the background, but not so large as to exclude all pixels in the light or dark spots. After ATP removal, there was a gradual decline in N_a (Figure 2C). The decline was not observed when ATP was maintained (Figure 2, D–F). The average N_a in three 4-s intervals 1) before the switch, 2) immediately after the switch, and 3) 55 s after the switch are compared in Figure 3. By 55 s after ATP removal, N_a had decreased by 72%. No significant change was seen if ATP was maintained.

The second analysis confirmed that the removal of ATP reduced granule motion. Motions of individual granules were tracked and averaged in 10-s intervals immediately before and 50–60 s after the switch. The ratio of the mean

Figure 2 (facing page). Difference-image analysis of granule movement before and after removal of ATP. Chromaffin cells were labeled with transiently expressed ANP-GFP, which targets to the secretory granule. Cells were visualized by TIRFM and followed for 20 s before being permeabilized for 30 s with 20 μM digitonin in NaGEP buffer containing 2 mM MgATP, incubated for an additional 60 s in the continuing presence of MgATP, and finally incubated for 60 s in the absence (A–C) or presence (D–F) of MgATP. These movies were subjected to difference-image analysis. Each image was subtracted from the subsequent image on a pixel by pixel basis. A dark spot indicates a negative change (i.e., the disappearance of a granule), an example of which is circled in black in A. A bright white spot (white circle in A) indicates a positive change. A black/white pair (adjacent to white arrow, A) indicates a granule moving laterally, in the direction of black to white (direction indicated by white arrow). (C and F) For each difference-image, the number of pixels above a threshold (or below a negative threshold) was counted. Threshold values were large enough to exclude pixel differences that were in the background, but not so large as to exclude all pixels in the light or dark spots. Asterisks in C and F mark the location of the individual difference-images shown in A and B and D and E, respectively. Bar, 5 μm.

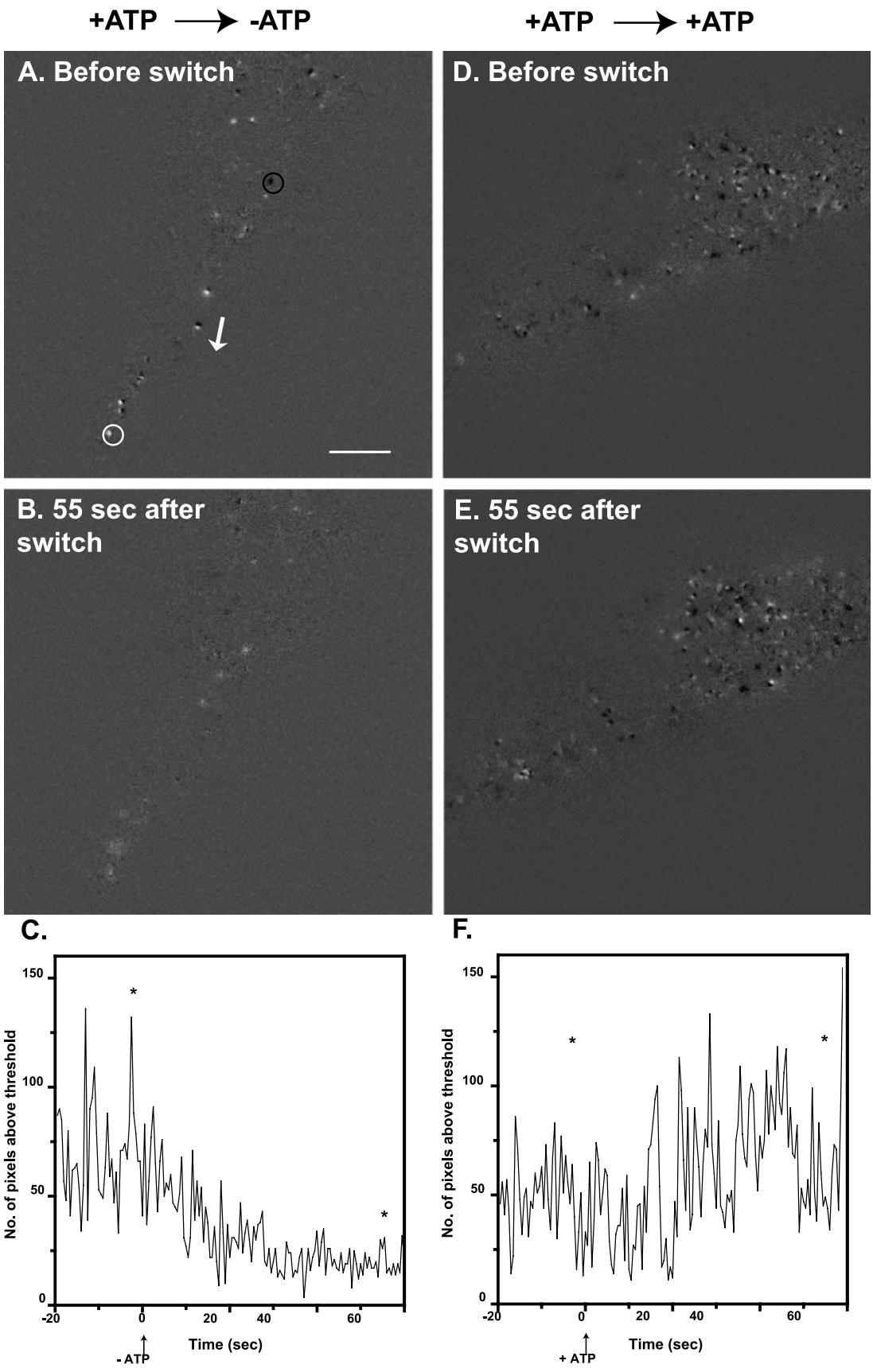
+ATP → -ATP
+ATP → +ATP
A. Before switch
D. Before switch
B. 55 sec after switch
E. 55 sec after switch
C.
F.
No. of pixels above threshold
150
100
50
0
-20
0
20
40
60
Time (sec)
- ATP
+ ATP
*

Figure 2.

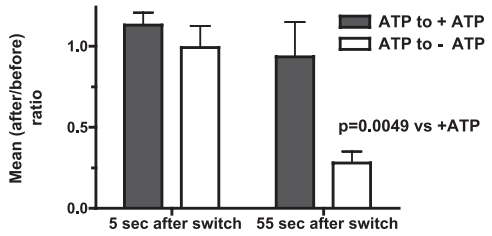

Figure 3. Summary of difference-image analysis. The number of pixels above a threshold (or below a negative threshold) was counted and averaged over three eight-frame intervals: 4 s before the removal of ATP, 4 s immediately after the switch to −ATP, and eight frames taken 55 s after the switch. For each cell, (after/before) ratios were calculated comparing the mean number of pixels greater than the threshold *after* the switch (either 5 or 55 s) to the mean number of pixels greater than the threshold *before* the switch. Thus each cell served as its own control. Student's *t* test was performed on the logarithms of the ratios (n = 6 cells/group). The logarithms were used (rather than the ratios themselves) since the ratio is an intrinsically asymmetrical measure and the logarithmic transformation is approximately Gaussian.

motion after/before was calculated for each granule (Figure 4A). After ATP removal, granules on average decreased their R motion by 17% ($p = 1 \times 10^{-5}$). 61% (70 of 114) of the tracked granules decreased their average motion. Granule motions in cells in which ATP was maintained during the solution switch had an average after/before ratio of 1.083; only 39% (69 of 177) of these granules decreased their motion. Motion in the *z* direction (toward or away from the plasma membrane) was also decreased upon ATP removal ($p = 2 \times 10^{-4}$) (Figure 4B).

A larger effect of ATP removal was seen when we examined a subpopulation of the granules that were especially slow-moving in the lateral plane. Here, there was a strong tendency for the slowest granules (mean $\Delta R_{before} < 10$ nm) to *increase* their motion over time in the presence of ATP, but not in its absence (Figure 4C).

The effects of ATP removal on motion were smaller when individual granules were tracked than when analyzed by the image-difference method (compare Figures 3 and 4). This difference probably resulted from different granules being analyzed. The tracking method analyzed motions of only those granules that remained in the evanescent field (moved less than ~200 nm in the *z* direction) for the duration of the measurement. Granules that move large distances (more than ~200 nm) into the cell interior (*z* direction) become so faint that they can no longer be tracked and are thus excluded from this analysis. The difference-image method highlights these granules. In addition, the relative effect of ATP removal in the difference-image method is dependent upon the chosen threshold.

Nicotinic Stimulation Increases Granule Motion in a Ca^{2+}-dependent Manner

Ca^{2+} not only triggers exocytosis but also enhances upstream ATP-dependent priming (Bittner and Holz, 1992; von Rüden and Neher, 1993). The possibility that stimulation alters granule motion before fusion was investigated. Chromaffin granules were labeled with VAMP-GFP, which gives a distinct fluorescent signature upon granule fusion with the plasma membrane (Allersma *et al*., 2004). Cells were perfused with control solution and then with solution containing the nicotinic agonist DMPP.

The distinct signature of fusion obtained with VAMP-GFP–labeled granules permits timing of the beginning of the fusion event to within 0.1–0.2 s (Allersma *et al*., 2004). The *z* and *R* motions of individual granules that underwent secretion were averaged and noise corrected during two 1-s intervals (10 Hz, frame acquisition) before stimulation (B1 and B2) and then during a 1-s interval 1.2–0.2 s before exocytosis (A). Ratios of the mean motions immediately before exocytosis to those before stimulation (A/B2) were calculated for each granule. To determine changes in motion unrelated to stimulation, B2/B1 ratios were calculated. The data are presented as histograms of the relative frequency of the ratios (Figure 5, A and B). There was an increase in motion upon stimulation. For example, the frequencies of *z* and *R* motion ratios greater than 2 were higher and those <2 were lower immediately before fusion compared with the prestimulation period. The median values increased from 0.81 and 0.96 to 1.27 and 1.22 for *z* and *R* motion ratios, respectively.

Changes in motion of granules not destined to undergo exocytosis during stimulation were also investigated. In this experiment, the Ca^{2+} dependency of motion was examined. Granules were tracked for two 1-s intervals before stimulation (B1 and B2), for a 1-s interval during perfusion with DMPP in the absence of Ca^{2+} (A1) and then for a 1-s interval with DMPP in the presence of Ca^{2+} (A2). Ratios of the mean motions during stimulation with DMPP to before stimulation (A1/B2 and A2/B2) were calculated for each granule. There was considerable variability in the motions during the intervals and in the ratios of the mean motions for individual granules. The effects of stimulation in the large population of granules (330 granules) not undergoing secretion were smaller than in the population of fusing granules (59–84 granules; see Figure 5 legend). Nevertheless, statistically significant, Ca^{2+}-dependent increases in motion were

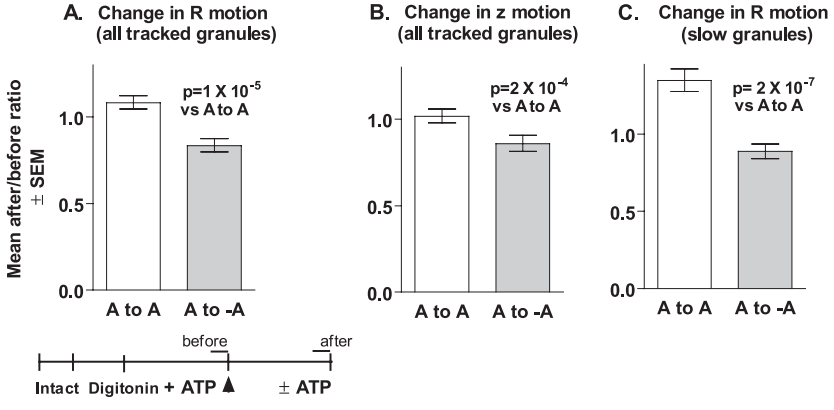

Figure 4. Tracking granule motions before and after removal of ATP. The movements of individual granules in the cells from Figure 3 were tracked for twenty frames (2 Hz) before and after the removal of MgATP, and ratios [mean motion after/mean motion before] were calculated for each tracked granule. (A) Change in lateral (*R*) motion for all tracked granules. ATP to ATP, n = 177; ATP to no ATP, n = 114. (B) Change in *z* motion for all tracked granules. (C) Change in *R* motion for granules with mean $\Delta R_{before} < 10$ nm. ATP to ATP, n = 72; ATP to no ATP, n = 69.

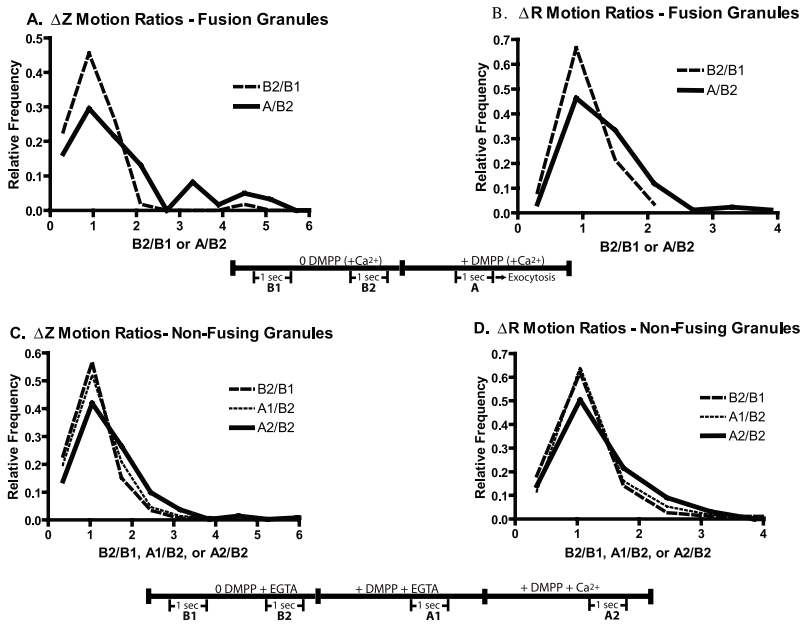

Figure 5. Nicotininc stimulation causes Ca^{2+}-dependent increases in granule motion. Chromaffin cells were transiently transfected with a plasmid encoding VAMP-GFP, which labels secretory granules. (A and B) Cells were visualized with TIRFM for 5 s before stimulation with the nicotinic agonist DMPP in the presence of 2.2 mM Ca^{2+}. The noise-corrected *z* and *R* motions of individual granules that underwent secretion were determined during two 1-s intervals (10 Hz, frame acquisition) before stimulation (B1 and B2) and then during a 1-s interval 1.2–0.2 s before exocytosis. Ratios of the mean motions immediately before exocytosis to that before stimulation (A/B2) were calculated for each granule. Changes in motion unrelated to stimulation, B2/B1 ratios, were also determined. Motions of 59 granules in *z* and 84 granules in *R* from 19 cells were calculated. The numbers were limited to granules that could be tracked from the beginning of the experiment with motions at least twice the estimated noise. The distributions of the ratio of motions are significantly different for A/B2 versus B1/B2 for Δz and ΔR ($p < 0.003$ and 0.0001, respectively, Mann–Whitney *U* test). (C and D) Effects of nicotinic stimulation on granules not undergoing exocytosis were investigated. Cells were bathed in Ca^{2+}-free PSS with 0.1 mM EGTA and sequentially perfused with Ca^{2+}-free PSS with 2 mM EGTA (including intervals B1 and B2), 20 μM DMPP without Ca^{2+} + 2 mM EGTA (including interval A1), and finally with 20 μM DMPP + 10 mM Ca^{2+} (including interval A2). Noise-corrected Δz and ΔR motions of greater than 330 individually tracked granules from 13 cells were determined. Mean motions during each of the 1-s intervals were determined and the indicated ratios were calculated. $p < 0.001$ for the distributions of both Δz and ΔR ratios of A2/B2 versus B2/B1 (Mann–Whitney *U* test).

detected (Figure 5, C and D). Median values of the ratios increased from 1.00 during the control intervals (B2/B1) to 1.17 (A2/B2) for both *z* and *R* motions.

Motion of Granules in the Evanescent Field before Exocytosis

Most granules that underwent exocytosis were present in the evanescent field for many seconds to minutes. The motion of these granules immediately preceding exocytosis was investigated to determine changes that might reflect a commitment to fusion.

Because instrumental noise (shot noise and CCD readout noise) could be misinterpreted as motion, noise as a function of granule intensity was measured experimentally on immobilized fluorescent beads, and the results were incorporated into the corrections on chromaffin cell granule data (see Appendix). The analysis was applied to individual granule measurements in the four 100-ms intervals before fusion (Figure 6). The z motions were compared for alternating 100-ms intervals so as to avoid negative correlation artifacts (see Appendix). The analysis defined, with a 95% confidence, measurements that could be not accounted for by noise. These measurements are presented in Figure 6 and represent 50% of all of the fusion events for which granules could be tracked for 400 ms before fusion. All but two of the ~70 granules are represented in both A and B. Ninety percent of the granules in each panel had significant motion during both intervals (open black squares) with the remainder having significant motion in one of the two intervals (red triangles). Thus, half of the granules undergo significant motion within a few hundred milliseconds of fusion. The other half of the granules had motions too small to be distinguished from measurement noise. These granules could either be immobile or undergoing very small motions. R motions were also significant and varied from tens to hundreds of nanometers (Figure 6, C and D). Some granules moved greater than 200 nm during the last 100 ms before fusion (Figure 6D, Δ_{-1} axis).

There was no preference for movement toward (negative direction) or away from (positive direction) the glass interface during intervals −4 through −2. However, in the ultimate interval (−1) before fusion there were more motions toward the glass interface than away (49 versus 13) among those granules with significant motions (Wilcoxon signed rank test, $p < 0.001$). However, this potentially significant finding is subject to ambiguity. An increase in granule intensity may be caused, not only by motion toward the plasma membrane, but also by capturing the beginning of a fusion event, with brightening due to the effect of increased pH on EGFP fluorescence. The interpretation of these data is limited by the accuracy with which we can identify the beginning of the fusion event.

We previously found that 20% of the granules that undergo exocytosis were not evident in the evanescent field within 100–300 ms of fusion (Allersma *et al.*, 2004). Most of the granules that suddenly appeared had sufficient amounts of VAMP-GFP to have been detected if they had been present within the evanescent field. We have further refined the analysis by selecting granules that were invisible in the evanescent field and had especially bright postfusion VAMP-GFP fluorescence (see Figure 7 for examples). The analysis shows that 6% of all fusion events involve granules that were undetected immediately before exocytosis and yet displayed a postfusion fluorescence greater than the median of granules that were present in the evanescent field before exocytosis. Granules not undergoing exocytosis rarely move into or out of the evanescent field. In random 0.3-s intervals; <1% of the granules did so. The 6% of the fusion events corresponding to granules that suddenly arrived at and fused with the plasma membrane is many times larger than one would expect by chance.

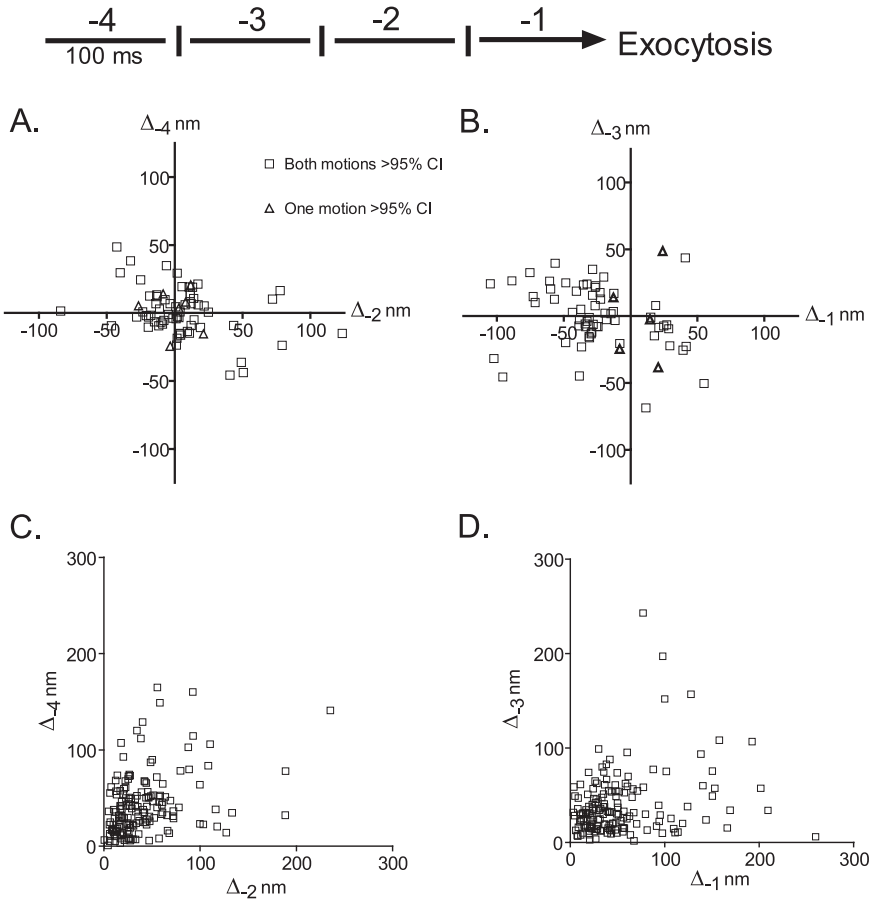

Figure 6. The last four granule motions before fusion. The motions of 159 granules before fusion were determined. (A and B) The *z* motions are shown during intervals −4 and −2, and during intervals −3 and −1, respectively, before exocytosis. Motions toward the glass interface are negative. Motions are shown for which one or both of the pair has or have greater than a 95% probability of not being accounted for by instrumental noise (see Appendix). Both measurements were at greater than 95% confidence intervals for 63 and 62 granules in A and B, respectively. (C and D) The *R* motions are shown during intervals −4 and −2, and during intervals −3 and −1, respectively, before exocytosis. All *R* motions were statistically significant at the 95% confidence interval.

Granule and Plasma Membrane Motion

The z motions relative to the glass interface could reflect individual granule motions to and from the plasma membrane or coupled granule and plasma membrane motion. If plasma membrane motions cause *z* motions, then motions of nearby granules are likely to be correlated. This was not the case (Table 1). The correlation of granule motions was essentially zero for granules almost immediately adjacent to each other (<0.5 μm apart) as well as for granules further apart. Simulations of random motions including instrumental noise showed that the granule cross-correlations displayed in Table 1 are consistent with adjacent granules moving with <2% coupling.

Granule Motion and Actin

The region illuminated by TIRFM in chromaffin cells contains a well-formed actin cytoskeleton (Nakata and Hirokawa, 1992). It is generally assumed that this cortical actin network is responsible for the restricted granule motion. One effective method of reducing cortical F-actin is by reducing plasma membrane phosphatidylinositol-4,5-bisphosphate (PtdIns-4,5-P_2) through removal of ATP (Bittner and Holz, 2005). However, as reported above, removal of ATP reduced rather than increased granule motion. Because removal of ATP could have multiple effects, we examined the effects on granule motion of two specific actin reagents—latrunculin B and YpkA. Latrunculin B binds soluble G-actin and alters the F-actin:G-actin equilibrium, thereby causing F-actin disassembly in vitro and in cells in which actin is rapidly turning over. We recently found that cortical actin in chromaffin cells is resistant to disruption by latrunculin B and functionally related drugs (Bittner and Holz, 2005). Nevertheless, there may have been effects of latrunculin B on the actin cytoskeleton that were not visualized by light microscopy because latrunculin B did alter secretion. YpkA is a protein kinase expressed by *Yersinia* that is activated by and phosphorylates actin. It causes disassembly of actin stress fibers in epithelial cells (Juris *et al*., 2000). YpkA strongly reduces cortical actin and inhibits secretion in chromaffin cells (Bittner and Holz, 2005).

Because intact cells but not permeabilized cells round up upon incubation with latrunculin, granule motion was investigated in the latter. Changes in granule motion were analyzed using a number of different approaches. Individual granules were tracked for 20-s intervals before and after perfusion with latrunculin B, and the ratio of the averages of the motions in the two intervals was calculated. Latrunculin B did not have a significant effect on *R* or *z* motions (Table 2). Analysis of difference images (similar to Figure 2) also showed no consistent effect of latrunculin B (our unpublished data). Latrunculun B also did not alter the average of all the motions nor the relative number of large motions in the cell (*R* motions ≥25 nm). Thus, using a variety of different analyses, we could not demonstrate a significant change in granule motion caused by latrunculin B.

YpkA was transiently expressed in chromaffin cells; thus, it was impossible to track individual granules before and after YpkA. We asked whether the expression of YpkA caused a large and generalized increase in granule motion. YpkA expression did not remove restrictions on granule

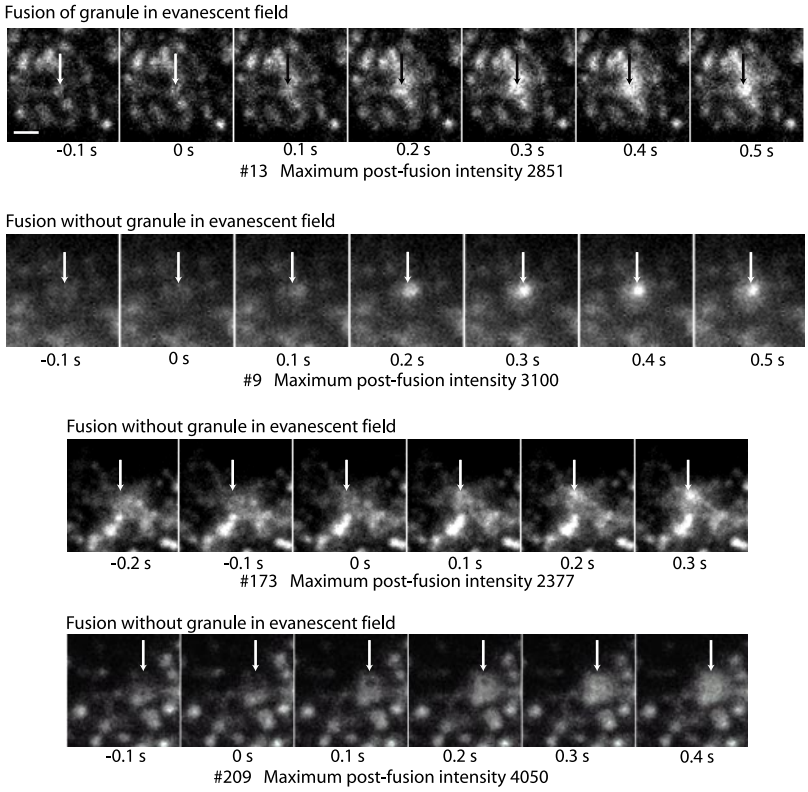

Figure 7. Fusion can occur without the granule occurring in the evanescent field. Three events are shown (9, 173, and 209) in which fusion occurs with the granule not evident in the evanescent field within 100 ms of the event. For comparison, event 13 (top sequence) shows a granule in the evanescent field immediately before fusion. Images were taken at 10 Hz. Zero time is the frame just before the fusion event that is characterized by spreading and increase in the intensity. The arrows indicate the position of the fusion event and are identically placed in the frames within a sequence. The maximum postfusion intensity (in arbitrary units; a.u.) reflects the total amount of VAMP-GFP in the granule after it is exposed to the extracellular medium at pH 7.4. The median postfusion fluorescence of granules that were present in the evanescent field before fusion was 2000 a.u. Note that event 9 shows a hint of an out-of-focus granule at −0.1 and 0 s. The out-of-focus granule is probably visualized because of a small amount of contaminating propagated light caused by spurious reflections in the objective lens (Mattheyses and Axelrod, 2006) and/or interaction of the evanescent field with highly refractive intracellular structures (Oheim and Stuhmer, 2000). Bar, 1 μm.

motion. For example, mean *R* motions in cells expressing and not expressing YpkA were 19.4 ± 2.8 and 20.1 ± 3.1, respectively (6 or 4 cells/group; 24,000 motions/group).

DISCUSSION

Numerous studies using TIRFM in primary neuroendocrine cells demonstrate that the motions of the majority of granules that are immediately adjacent to the plasma membrane are highly restricted, with granules moving many orders of magnitude less than predicted for free diffusion. In chromaffin cells, <1% of granules move more than a granule diameter in several seconds or more than 1 μm in 4 min (Johns *et al*., 2001). The jittering suggests that granules are either caged or tethered. The current study was undertaken to better understand the relationship of this restricted motion to exocytosis. It has three major findings: 1) the highly restricted motion is itself regulated by ATP and Ca^{2+}, both of which play critical roles in secretion; 2) significant granule motion often immediately precedes fusion with the plasma membrane; and 3) disruption of F-actin and actin dynamics is not associated with an increase in granule motion. These issues are discussed below.

The Highly Restricted Motion of Granules Is Regulated by ATP and Ca^{2+}

Because granule motions in primary secretory cells are small and variable, it has been difficult to study their regulation.

Table 1. The *z* motions of neighboring granules are not correlated

Separation (μm)	Correlation rho	No. of motions	No. of unique pairs
0.5	−0.069	597	37
0.78	0.009	13,404	227
1.0	−0.006	36,159	473
2.0	0.001	173,849	1827
3.0	0.004	332,742	3398

A Pearson's correlation rho was calculated between pairs of z motions for granules in 21 cells. Rho = 1.0 or −1.0 signifies maximal correlation or inverse correlation, respectively. Rho = 0 indicates no correlation. The motions were almost completely uncorrelated, even for granules that were side by side (0.5-μm distance).

Table 2. Latrunculin B does not alter motion of tracked granules

	Control ratio of motions	No. of motions	Latrunculin B ratio of motions	No. of motions
R motions	1.05 (0.96–1.15)	3200	1.11 (1.00–1.22)	1800
z motions	1.05 (0.97–1.13)	3200	1.04 (0.93–1.17)	1800

The effects of latrunculin B on the motion of individual, tracked granules labeled with ANP-GFP were determined. Cells were subjected to perfusion with three solutions as follows: 1) intact cells, no digitonin, no latrunculin B (20 s) →; 2) permeabilization, digitonin ± latrunculin B (10 μM) (30 s) →; and 3) no digitonin in the continuing presence or absence of latrunculin B (60 s). The movements of individual granules were tracked for 20 s (2 Hz) before permeabilization (incubation 1) and at the end of incubation 3, and ratios [mean motion in 3/mean motion in 1] were calculated for each tracked granule. The motions of 80 and 45 granules were tracked in control and latrunculin B-treated cells, respectively. A ratio of greater than one indicates an increase in motion. The numbers in parentheses are the 95% confidence intervals.

We devised a number of methods in which each cell or each individual granule serves as its own control. We found that ATP maintains, and nicotinic agonist-induced Ca^{2+} influx increases, the small motions observed in TIRFM. An important conclusion from these studies is that the characteristic small motions of granules reflect regulated processes.

The tracking of individual granules revealed that the slowing caused by ATP removal resulted in part from the loss of a normally occurring increase in motion of slower moving granules (Figure 4). This finding is consistent with a role for a motor protein in maintaining the jittering motion. Indeed, chromaffin granules are associated with myosin Va (Wang and Holz, unpublished observations), and myosin II is concentrated adjacent to the chromaffin cell plasma membrane (Neco *et al*., 2002, 2004). Both motors have been implicated in secretion (Neco *et al*., 2002, 2004; Desnos *et al*., 2003; Waselle *et al*., 2003; Varadi *et al*., 2005). Some of the motions were of the order of the 5- to 10-nm unitary steps of myosin II (Murphy *et al*., 2001; Veigel *et al*., 2003) and the 37-nm unitary steps of myosin Va (Mehta *et al*., 1999; Vale, 2003; Yildiz *et al*., 2003) observed in vitro. Because both myosin II and myosin Va are regulated by Ca^{2+}, it is possible that the effects of ATP and Ca^{2+} on granule motion are through these molecular motors.

Both ATP (Holz *et al*., 1989; Bittner and Holz, 1992; Hay and Martin, 1992; Parsons *et al*., 1995) and Ca^{2+} (Bittner and Holz, 1992; von Rüden and Neher, 1993) prime chromaffin cells to undergo secretion before the final Ca^{2+} trigger. The ability of these cofactors to increase granule motion in the immediate vicinity of the plasma membrane may reflect a pathway through which ATP and Ca^{2+} prime secretion. Such a pathway might involve plasma membrane PtdIns-4,5-P_2, which is maintained by ATP (Eberhard *et al*., 1990; Hay *et al*., 1995) and increased by micromolar Ca^{2+} in chromaffin cells (Eberhard and Holz, 1991). PtdIns-4,5-P_2 is a key membrane lipid involved in the priming and regulation of exocytosis (Eberhard *et al*., 1990; Hay *et al*., 1995). It serves as a cofactor for many proteins involved in vesicle trafficking and is necessary for the maintenance of cortical actin in chromaffin cells (Bittner and Holz, 2005). The lipid could play a role in regulating the motion together with or independently of motor proteins.

The regulation of granule motion in chromaffin cells by ATP and Ca^{2+} has precedents. Removal of ATP also reduces granule motion adjacent to the plasma membrane in PC12 cells (Lang *et al*., 2000) and repetitive, high-frequency depolarization in the presence of Ca^{2+} stimulates granule motion in *Drosophila* neurons viewed by wide-field epifluorescence microscopy (Shakiryanova *et al*., 2005).

Significant Granule Motion Occurs within 100 ms of Fusion Suggests Transient Granule/Plasma Membrane Interaction before Fusion

We find that granule motion, although restricted, nevertheless can be significant immediately before exocytosis. The *z* motions (measured by granule intensity changes in the exponentially decaying evanescent field) are occasionally 50–150 nm within 0.1–0.2 s of fusion, although usually less. The *R* motions (measured by tracking the granule center) are often 50–200 nm within 0.1–0.2 s of fusion. Furthermore, in a previous study ~20% of the fusion events were not associated with an antecedent granule in the evanescent field (Allersma *et al*., 2004). Here, we show that 6% of all fusion events involved granules that were not apparent in earlier frames and were also above average in brightness immediately after exocytosis. This result is consistent with some granules having traveled several hundred nanometers toward the plasma membrane during the last 100 ms before fusion (Allersma *et al*., 2004). However, it is also consistent with an alternative possibility: some fusion events may occur at narrow invaginations of the plasma membrane extending deep into the cytosol. Double-label experiments designed to simultaneously monitor the granule and the local plasma membrane morphology should resolve this ambiguity.

Studies in other cells also indicate that granules undergo motion shortly before fusion. Mobile rather than immobile granules in growth cones of PC12 cells have a greater probability of undergoing exocytosis (Burke *et al*., 1997). Fusion is not preceded by a reduction in mobility within 0.5 s of fusion (Ng *et al*., 2003). Mobile protein-containing granules undergo exocytosis in presynaptic boutons of the neuromuscular junction in *Drosophila* (Shakiryanova *et al*., 2005). Similarly, granule motion in growth cones of hippocampal neurons is significant within 0.5 s of fusion (Silverman *et al*., 2005). Vesicle motion is also important for fast release in at least some neurons. Fast, tonic neurotransmitter release at the ribbon synapse in the inner hair cell neuron requires continuous and rapid vesicle replenishment from remote regions in the cell with vesicle residence times release sites of 100 milliseconds or less (Griesinger *et al*., 2005).

The observations that granules can move shortly before fusion contrast with the common assumption that granules that are morphologically close to the plasma membrane (within a granule diameter) are stably interacting with the membrane and that this bound state is required for priming and subsequent exocytosis (Figure 8, standard model). Some of the granules adjacent to the plasma membrane that undergo exocytosis are mobile within 0.1 s of fusion. How then might priming of the pathway occur? A well-established priming condition (discussed above), the maintenance of plasma membrane PtdIns-4,5-P_2 by ATP (Eberhard *et al*., 1990; Hay *et al*., 1995; Holz *et al*., 2000), does not directly involve the secretory granule and therefore can occur without the granule interacting with the plasma membrane. Other steps involving the interaction of the granule with the plasma membrane may be able to occur rapidly.

Although the majority of the motions were less than the diameter of a chromaffin granule, they are much greater than electrostatic, van der Waals, or hydrogen bond distances (all <0.5 nm). Many are also greater than the likely 12- to 24-nm length of a partially zippered, quaternary, trans-soluble *N*-ethylmaleimide-sensitive factor attachment protein receptor (SNARE) complex (Sutton *et al*., 1998). The distinction between being adjacent to and being bound to the plasma membrane has important consequences. Our data imply that the interaction of granule and plasma membrane SNAREs that leads to exocytosis must be able to occur within 100 ms of fusion (but see Coorssen *et al*., 1998) for an upstream function for SNAREs. Indeed, rapid interactions between synaptic vesicles and the plasma membrane must be occurring in the very fast events associated with synaptic transmission in inner hair cells (Griesinger *et al*., 2005). The data are also consistent with the notion that the interaction of granule membrane and plasma membrane proteins are dynamic and reversible, as was suggested in a previous study in which the effects on granule position of cleavage of SNARE proteins by clostridial neurotoxins were investigated (Johns *et al*., 2001).

Granule motion adjacent to the plasma membrane may increase the probability of exocytosis. Small motions may permit granules adjacent to the plasma membrane to re-

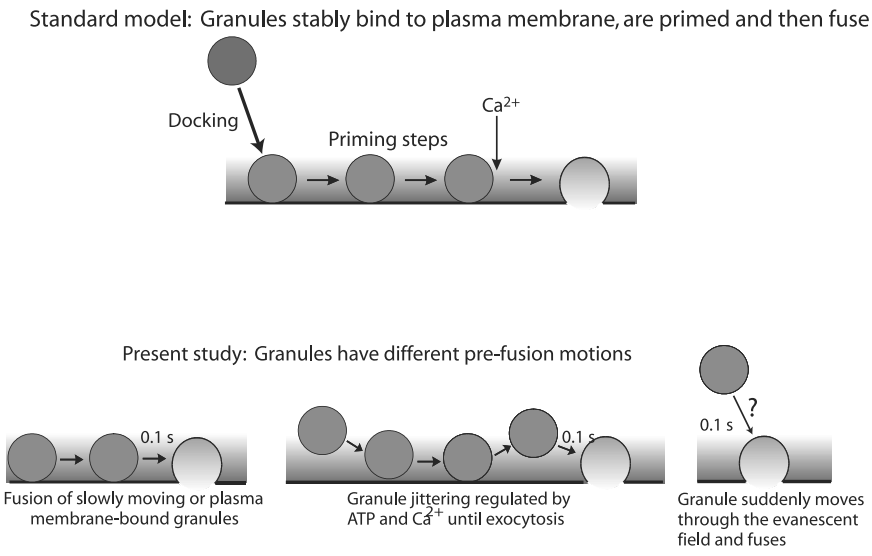

Figure 8. Behavior of granules before exocytosis. A standard model for exocytosis is that granules translocate from the cell interior to the plasma membrane and stably bind or dock to the plasma membrane. After subsequent priming steps, the granule is able to fuse with the plasma membrane in respond to elevated Ca^{2+}. The present study indicates that granules that undergo exocytosis can have numerous behaviors immediately preceding fusion. Some granules do not undergo detectable motion and may be bound to the plasma membrane. Others are jittering in place within 100 ms of fusion. A few granules are not present in the evanescent field before fusion and may move through it within 100 ms of fusion. Granule and plasma membrane priming events can occur before the final docking step that leads to fusion.

petitively sample microdomains of the plasma membrane, thereby increasing the probability of fruitful interactions that lead to fusion. The initial burst of exocytosis in chromaffin cells upon flash photolysis of caged Ca^{2+} (a total of ~200 granules) (Voets, 2000) reflects the fraction of the ~1000 granules within a granule diameter of the plasma membrane that are favorably interacting with the plasma membrane during the Ca^{2+} stimulus. The duration of the initial burst, ~0.5 s, is sufficient time for the jittering motions to randomly sample the fusion environment on the plasma membrane and thereby influence the rapid kinetics of secretion from the chromaffin cell.

Granule Motion and Actin

There are two ways in which the actin cytoskeleton might affect secretory granule motion, and evidence exists that supports both ways. Granules might be tethered to or caged by actin, restricting their motion. Consistent with this is the observation that granule motion is indeed restricted (Oheim *et al.*, 1998; Han *et al.*, 1999; Steyer and Almers, 1999; Johns *et al.*, 2001). Further support for this notion comes from a study in which mycalolide B, which like latrunculin B can bring about the depolymerization of F-actin, increased granule mobility in the *processes* of differentiated PC12 cells (Ng *et al.*, 2002). Conversely, actin might be required for some granule motions, either by serving as a track for molecular motors or for the generation of actin comets. This would be consistent with studies which suggest that latrunculin decreases granule mobility in PC12 cells (Lang *et al.*, 2000) and acridine orange labeled vesicles in chromaffin cells (Oheim and Stuhmer, 2000).

The experiments in the present work follow a study from our laboratory concerning the regulation of the cortical actin cytoskeleton in chromaffin cells (Bittner and Holz, 2005). We found that the cortical actin cytoskeleton in these primary, nondividing cells is relatively resistant to G-actin-binding drugs such as latrunculin B and mycalolide B. Thus, the absence of effects of latrunculin B on granule motion does not allow us to draw conclusions about granule motion after actin disassembly. They do suggest, however, that dynamic G-actin-dependent reactions are not required for the jittering granule motion during the short duration of the experiments.

There were two situations in which we know that actin *was* disassembled. One was during incubation in the absence of ATP, and the other is in cells expressing YpkA. Most notably, neither removal of ATP nor the expression of YpkA increased granule motion. Indeed, removal of ATP resulted in a *decrease* in motion. The results argue against the actin cytoskeleton acting as a passive impediment for granule motion. Either very little F-actin is required to restrict the motion of granules, or factors other than cortical actin limit granule motion in the resting cell. The mechanisms underlying the restricted motion of granules adjacent to the plasma membrane remain an important subject for future investigation.

Variability of Granule Motion

Granules close to the plasma membrane showed heterogeneity in response to experimental interventions. ATP and nicotinic stimulation evoked changes in motion of only a small fraction of the total number of granules visualized in the evanescent field. ATP increased the motion primarily of the subpopulation of especially slow moving granules and not of all of the granules. Similarly, only a small fraction of the granules increased their motion in response to nicotinic stimulation. The basis for the heterogeneity is unknown, but may relate to the different ability of neighboring granules to undergo exocytosis.

We also found that granule motions varied from cell to cell. The percentage of granules moving greater than 25 nm in R varied from 5 to 50% among cells. This characteristic was stable in that it persisted after the cells were permeabilized with digitonin (Bittner and Holz, unpublished observations). The basis for the variability and its significance in secretion remain to be determined.

Measurement Noise in TIRFM Experiments

In addition to the biological insights into granule motion and exocytosis, this study is notable because of the development of image analysis and statistical techniques to distinguish between the small granule motions in living cells and instrumental noise. Instrumental noise has two effects: 1) it leads to an overestimate in the calculated mean frame-to-frame motion; and 2) it increases the uncertainty of the calculated mean for average motion, even after correction for the overestimate of the mean. In our case, we find that

most of the instrument noise is CCD readout noise (including dark count noise) rather than shot noise. This is good news for future studies, because the new generation of electron-multiplying CCD cameras greatly reduces the effective readout noise at low light levels.

ACKNOWLEDGMENTS

We thank Drs. Li Wang (University of Michigan) and Edwin S. Levitan for helpful discussions. This work was funded by National Institutes of Health Grants R01-DK50127 (to R.W.H.), R01-NS38129 (to D. A.), and a Michigan Economic Development Corporation and the Michigan Life Sciences Corridor Grant (to R.W.H.).

REFERENCES

Allersma, M. W., Wang, L., Axelrod, D., and Holz, R. W. (2004). Visualization of regulated exocytosis with a granule-membrane probe using total internal reflection microscopy. Mol. Biol. Cell *15*, 4658–4668.

Axelrod, D. (1981). Cell-substrate contacts illuminated by total internal reflection fluorescence. J. Cell Biol. *89*, 141–145.

Axelrod, D. (2001). Selective imaging of surface fluorescence with very high aperture microscope objectives. J. Biomed. Opt. *6*, 6–13.

Axelrod, D. (2003). Total internal reflection fluorescence microscopy in cell biology. Methods Enzymol. *361*, 1–33.

Axelrod, D., Burghardt, T. P., and Thompson, N. L. (1984). Total internal reflection fluorescence. Annu. Rev. Biophys. Bioeng. *13*, 247–268.

Bittner, M. A., and Holz, R. W. (1992). Kinetic analysis of secretion from permeabilized adrenal chromaffin cells reveals distinct components. J. Biol. Chem. *267*, 16219–16225.

Bittner, M. A., and Holz, R. W. (2005). Phosphatidylinositol-4,5-bisphosphate: actin dynamics and the regulation of ATP-dependent and independent secretion. Mol. Pharmacol. *67*, 1089–1098.

Burke, N. V., Han, W., Li, D., Takimoto, K., Watkins, S. C., and Levitan, E. S. (1997). Neuronal peptide release is limited by secretory granule mobility. Neuron *19*, 1095–1102.

Coorssen, J. R., Blank, P. S., Tahara, M., and Zimmerberg, J. (1998). Biochemical and functional studies of cortical vesicle fusion: the SNARE complex and Ca2+ sensitivity. J. Cell Biol. *143*, 1845–1857.

Desnos, C., *et al*. (2003). Rab27A and its effector MyRIP link secretory granules to F-actin and control their motion towards release sites. J. Cell Biol. *163*, 559–570.

Eberhard, D. A., Cooper, C. L., Low, M. G., and Holz, R. W. (1990). Evidence that the inositol phopholipids are necessary for exocytosis: loss of inositol phospholipids and inhibition of secretion in permeabilized cells caused by a bacterial phospholipase C and removal of ATP. Biochem. J. *268*, 15–25.

Eberhard, D. A., and Holz, R. W. (1991). Calcium promotes the accumulation of polyphosphoinositides in intact and permeabilized bovine chromaffin cells. Cell. Mol. Neurobiol. *11*, 357–370.

Griesinger, C. B., Richards, C. D., and Ashmore, J. F. (2005). Fast vesicle replenishment allows indefatigable signalling at the first auditory synapse. Nature 212–215.

Han, W., Ng, Y. K., Axelrod, D., and Levitan, E. S. (1999). Neuropeptide release by efficient recruitment of diffusing cytoplasmic secretory vesicles. Proc. Natl. Acad. Sci. USA *96*, 14577–14582.

Hay, J. C., Fisette, P. L., Jenkins, G. H., Fukami, K., Takenawa, T., Anderson, R. A., and Martin, T.F.J. (1995). ATP-dependent inositide phosphorylation required for Ca^{2+}-activated secretion. Nature *374*, 173–177.

Hay, J. C., and Martin, T.F.J. (1992). Resolution of regulated secretion into sequential MgATP-dependent and calcium-dependent stages mediated by distinct cytosolic proteins. J. Cell Biol. *119*, 139–151.

Holz, R. W., Bittner, M. A., Peppers, S. C., Senter, R. A., and Eberhard, D. A. (1989). MgATP-independent and MgATP-dependent exocytosis. Evidence that MgATP primes adrenal chromaffin cells to undergo exocytosis. J. Biol. Chem. *264*, 5412–5419.

Holz, R. W., Brondyk, W. H., Senter, R. A., Kuizon, L., and Macara, I. G. (1994). Evidence for the involvement of Rab3a in Ca^{2+}-dependent exocytosis from adrenal chromaffin cells. J. Biol. Chem. *269*, 10229–10234.

Holz, R. W., Hlubek, M. D., Sorensen, S. D., Fisher, S. K., Balla, T., Ozaki, S., Prestwich, G. D., Stuenkel, E. L., and Bittner, M. A. (2000). A pleckstrin homology domain specific for PtdIns-4-5-P_2 and fused to green fluorescent protein identifies plasma membrane PtdIns-4-5-P_2 as being important in exocytosis. J. Biol. Chem. *275*, 17878–17885.

Ivarsson, R., Obermuller, S., Rutter, G. A., Galvanovskis, J., and Renstrom, E. (2004). Temperature-sensitive random insulin granule diffusion is a prerequisite for recruiting granules for release. Traffic *5*, 750–762.

Johns, L. M., Levitan, E. S., Shelden, E. S., Holz, R. W., and Axelrod, D. (2001). Restriction of secretory granule motion near the plasma membrane of chromaffin cells. J. Cell Biol. *153*, 177–190.

Juris, S. J., Rudolph, A. E., Huddler, D., Orth, K., and Dixon, J. E. (2000). A distinctive role for the *Yersinia* protein kinase: actin binding, kinase activation, and cytoskeleton disruption. Proc. Natl. Acad. Sci. USA *97*, 9431–9436.

Lang, T., Wacker, I., Wunderlich, I., Rohrbach, A., Giese, G., Soldati, T., and Almers, W. (2000). Role of actin cortex in the subplasmalemmal transport of secretory granules in PC-12 cells. Biophys. J.*78*, 2863–2877.

Mattheyses, A. L., and Axelrod, D. (2006). Direct measurement of the evanescent field profile produced by objective-based TIRF. J. Biomed. Opt. *11*, 014006.

Mehta, A. D., Rock, R. S., Rief, M., Spudich, J. A., Mooseker, M. S., and Cheney, R. E. (1999). Myosin-V is a processive actin-based motor. Nature *400*, 590–593.

Murphy, C. T., Rock, R. S., and Spudich, J. A. (2001). A myosin II mutation uncouples ATPase activity from motility and shortens step size. Nat. Cell Biol. *3*, 311–315.

Nakata, T., and Hirokawa, N. (1992). Organization of cortical cytoskeleton of cultured chromaffin cells and involvement in secretion as revealed by quick-freeze, deep- etching, and double-label immunoelectron microscopy. J. Neurosci. *12*, 2186–2197.

Neco, P., Gil, A., Frances, M., Viniegra, S., and Gutierrez, L. M. (2002). The role of myosin in vesicle transport during bovine chromaffin cell secretion. Biochem. J. *368*, 405–413.

Neco, P., Giner, D., Viniegra, S., Borges, R., Villarroel, A., and Gutierrez, L. M. (2004). New roles of myosin II during the vesicle transport and fusion in chromaffin cells. J. Biol. Chem. *279*, 27450–27457.

Ng, Y. K., Lu, X., Gulacsi, A., Han, W., Saxton, M. J., and Levitan, E. S. (2003). Unexpected mobility variation among individual secretory vesicles produces an apparent refractory neuropeptide pool. Biophys. J. *84*, 4127.

Ng, Y. K., Lu, X., and Levitan, E. S. (2002). Physical mobilization of secretory vesicles facilitates neuropeptide release by nerve growth factor-differentiated PC12 cells. J. Physiol. *542*, 395.

Ohara-Imaizumi, M., Nakamichi, Y., Tanaka, T., Ishida, H., and Nagamatsu, S. (2002). Imaging exocytosis of single insulin secretory granules with evanescent wave microscopy. distinct behavior of granule motion in biphasic insulin release. J. Biol. Chem. *277*, 3805–3808.

Oheim, M., Loerke, D., Stuhmer, W., and Chow, R. H. (1998). The last few milliseconds in the life of a secretory granule. Docking, dynamics and fusion visualized by total internal reflection fluorescence microscopy (TIRFM). Eur. J. Biophys. *27*, 83–98.

Oheim, M., and Stuhmer, W. (2000). Tracking chromaffin granules on their way through the actin cortex. Eur. J. Biophys. *29*, 67–89.

Parsons, T. D., Coorssen, J. R., Horstmann, H., and Almers, W. (1995). Docked granules, the exocytic burst, and the need for ATP hydrolysis in endocrine cells. Neuron *15*, 1085–1096.

Shakiryanova, D., Tully, A., Hewes, R. S., Deitcher, D. L., and Levitan, E. S. (2005). Activity-dependent liberation of synaptic neuropeptide vesicles. Nat. Neurosci. *8*, 173–178.

Silverman, M. A., Johnson, S., Gurkins, D., Farmer, M., Lochner, J. E., Rosa, P., and Scalettar, B. A. (2005). Mechanisms of transport and exocytosis of dense-core granules containing tissue plasminogen activator in developing hippocampal neurons. J. Neurosci. *25*, 3095–3106.

Steyer, J. A., and Almers, W. (1999). Tracking single secretory granules in live chromaffin cells by evanscent-field fluorescence microscopy. Biophys. J. *76*, 2262–2271.

Steyer, J. A., Horstman, H., and Almers, W. (1997). Transport, docking and exocytosis of single secretory granules in live chromaffin cells. Nature *388*, 474–478.

Stout, A. L., and Axelrod, D. (1989). Evanescent field excitation of fluorescence by epi-illumination microscopy. Appl. Opt. *28*, 5237–5242.

Sutton, R. B., Fasshauer, D., Jahn, R., and Brunger, A. T. (1998). Crystal structure of a SNARE complex involved in synaptic exocytosis at 2.4 angstrom resolution. Nature *395*, 347–353.

Tsuboi, T., Zhao, C., Terakawa, S., and Rutter, G. A. (2000). Simultaneous evanescent wave imaging of insulin vesicle membrane and cargo during a single exocytotic event. Curr. Biol. *10*, 1307–1310.

Vale, R. D. (2003). Myosin V motor proteins: marching stepwise towards a mechanism. J. Cell Biol. *163*, 445–450.

Varadi, A., Tsuboi, T., and Rutter, G. A. (2005). Myosin Va transports dense core secretory vesicles in pancreatic MIN6 β-cells. Mol. Biol. Cell *16*, 2670–2680.

Veigel, C., Molloy, J. E., Schmitz, S., and Kendrick-Jones, J. (2003). Load-dependent kinetics of force production by smooth muscle myosin measured with optical tweezers. Nat. Cell Biol. *5*, 980–986.

Voets, T. (2000). Dissection of three Ca^{2+}-dependent steps leading to secretion in chromaffin cells from mouse adrenal slices. Neuron *28*, 537–545.

von Rüden, L., and Neher, E. (1993). A Ca-dependent early step in the release of catecholamines from adrenal chromaffin cells. Science *262*, 1061–1065.

Waselle, L., Coppola, T., Fukuda, M., Iezzi, M., El Amraoui, A., Petit, C., and Regazzi, R. (2003). Involvement of the Rab27 binding protein Slac2c/MyRIP in insulin exocytosis. Mol. Biol. Cell *14*, 4103–4113.

Wick, P. W., Senter, R. A., Parsels, L. A., and Holz, R. W. (1993). Transient transfection studies of secretion in bovine chromaffin cells and PC12 cells: generation of kainate-sensitive chromaffin cells. J. Biol. Chem. *268*, 10983–10989.

Wilson, S. P., Liu, F., Wilson, R. E., and Housley, P. R. (1996). Optimization of calcium phosphate transfection for bovine chromaffin cells: relationship to calcium phosphate precipitate formation. Anal. Biochem. *226*, 212–220.

Yildiz, A., Forkey, J. N., McKinney, S. A., Ha, T., Goldman, Y. E., and Selvin, P. R. (2003). Myosin V walks hand-over-hand: single fluorophore imaging with 1.5 nm localization. Science *300*, 2061–2065.

APPENDIX: INSTRUMENTAL NOISE IN THE ANALYSIS OF GRANULE MOTION

The measurements of integrated intensity fluctuations observed frame to frame from individual granules are affected not only by the actual motion of granules but also by instrumental noise, mainly photon shot noise and CCD camera readout noise and dark count noise. The instrumental noise has two effects on the estimation of $<(\Delta z)^2>$ or $<(\Delta R)^2>$, which are measures of the amount of z motion or R motion in the time duration of a camera frame interval. The first effect is an overestimate of $<(\Delta z)^2>$ or $<(\Delta R)^2>$, because some part of the fluctuations arise purely from instrumental noise: even an absolutely fixed granule would seem to be moving. This overestimation bias can be corrected as described below. The second effect is an increase in the statistical uncertainty of results for $<(\Delta z)^2>$ or $<(\Delta R)^2>$, even after correction for the overestimation bias. This effect is also evaluated below. Any quantitative conclusions based on noise analysis of intensity data must take these two effects into account, to correctly report unbiased results and also to correctly evaluate whether values for motions under different biological conditions are significantly different from each other or from zero.

The correction and assignment of uncertainties for $<(\Delta z)^2>$ and for $<(\Delta R)^2>$ are somewhat different from each other so they are described separately.

Overestimation Correction for $<(\Delta z)^2>$

The primed variables here refer to the observables (i.e., before correction for instrumental noise) and the unprimed variables refer to actual motion. The intensities in successive frames I_1 and I_2 are already assumed to be background-subtracted.

At any time i,

$$I_i' = I_0 e^{-z_i'/d} \tag{A1}$$

where z_i' is the *apparent* z position. In terms of the *actual* z position, we have

$$I_i' = \alpha I_0 e^{-z_i/d} \tag{A2}$$

where α is a random variable representing instrumental noise that fluctuates around $<\alpha> = 1$ at any particular intensity. The statistical behavior of random variable α in general is a function of mean intensity; its value and statistical behavior is essentially the same as the normalized intensities seen in the experiments on immobilized debris or beads, samples that have no actual motion. From Eqs. A1 and A2 evaluated at the times $i = 1, 2$ of two successive camera exposures and taking the ratio, we get

$$e^{-\Delta z'/d} = \frac{\alpha_2}{\alpha_1} e^{-\Delta z/d} \tag{A3}$$

where $\Delta z \equiv z_2 - z_1$ and likewise for $\Delta z'$. Taking the log of Eq. A3 gives

$$\frac{\Delta z'}{d} = \frac{\Delta z}{d} + \ln \alpha_2 - \ln \alpha_1 \tag{A4}$$

The three terms on the right are all random variables that are completely independent of each other. In such a situation, the variance of a sum (or difference) is the sum of the variances. Therefore, their variances all add to produce the variance of the quantity on the left:

$$\mathrm{var}\frac{\Delta z'}{d} = \mathrm{var}\frac{\Delta z}{d} + 2\ \mathrm{var} \ln \alpha \tag{A5}$$

Note that in general $\mathrm{var}\Delta z = <\Delta z^2> - <\Delta z>^2$, and likewise for $\mathrm{var}\Delta z'$, so

$$\left\langle \left(\frac{\Delta z'}{d}\right)^2 \right\rangle = \left\langle \left(\frac{\Delta z}{d}\right)^2 \right\rangle + 2\ \mathrm{var}(\ln \alpha) + \left\langle \frac{\Delta z'}{d} \right\rangle^2 - \left\langle \frac{\Delta z}{d} \right\rangle^2 \tag{A6}$$

If any unidirectional motion (say, favoring motion toward the membrane) underlies the random motions, the last two terms on the right each may be nonzero. However, the difference between them is very small, as can be shown by taking the mean values on each side of Eq. A4 and examining $<\ln\alpha_2> - <\ln\alpha_1>$. The extreme maximum value of $<\ln\alpha_2> - <\ln\alpha_1>$ for any two intensity ranges, as calculated from noise read on immobilized beads of varying intensities with our CCD detector system, is <0.06. This means that the misreporting of any mean unidirectional motion $<\Delta z>$ because of CCD instrumental noise will be $<6\%$ of the characteristic depth d. Consequently, the last two terms on the right side of Eq. A6 almost cancel each other and can be safely ignored, even in the presence of unidirectional motion.

Equation A6 can be further simplified in the case where the fluctuations in α around its mean value of unity are small, as can be checked from the relative size of frame-to-frame intensity fluctuations on immobile debris or beads. In that case, $\ln\alpha \approx \alpha - 1$, and the var $(\ln\alpha)$ factor in Eq. A6 becomes var α, giving the approximate result:

$$\left\langle (\Delta z')^2 \right\rangle = \left\langle (\Delta z)^2 \right\rangle + 2d^2\ \mathrm{var}(\alpha) \tag{A7}$$

Therefore, to calculate a particular granule's corrected $<(\Delta z)^2>$ from the uncorrected $<(\Delta z')^2>$, we measure a sequence of intensities on a debris/bead sample, normalize the sequence to the average intensity, calculate the variance, multiply by $2d^2$, and subtract this value from the uncorrected $<(\Delta z')^2>$. Note that this procedure must be done with α values measured on a debris/bead sample that has the same mean intensity as the granule.

Overestimation Correction for $<(\Delta R)^2>$

The values for $\Delta R'$ are determined by quadrature from the component measurements of $\Delta X'$ and $\Delta Y'$. Each of those readings contains a "real" motion (ΔX, ΔY) denoted as unprimed, and a "noise" motion ($\Delta\beta_x$, $\Delta\beta_y$). The noise motion is the motion inferred from measurements on immobilized beads of similar size and intensity to a granule:

$$\begin{aligned} \Delta X' &= \Delta X + \Delta\beta_x \\ \Delta Y' &= \Delta Y + \Delta\beta_y \end{aligned} \tag{A8}$$

The frame-to-frame fluctuations in ΔX and ΔY are presumed to be uncorrelated with each other and also uncorrelated with the two uncorrelated instrumental noise fluctuations $\Delta\beta_x$ and $\Delta\beta_y$. Therefore,

$$\begin{aligned} \mathrm{var}\ \Delta X' &= \mathrm{var}\ \Delta X + \mathrm{var}\ \Delta\beta_x \\ \mathrm{var}\ \Delta Y' &= \mathrm{var}\ \Delta Y + \mathrm{var}\ \Delta\beta_y \end{aligned} \tag{A9}$$

Because the means of each of the random variable distances are zero, we have

$$\begin{aligned} \left\langle (\Delta X')^2 \right\rangle &= \left\langle (\Delta X)^2 \right\rangle + \left\langle (\Delta\beta_x)^2 \right\rangle \\ \left\langle (\Delta Y')^2 \right\rangle &= \left\langle (\Delta Y)^2 \right\rangle + \left\langle (\Delta\beta_y)^2 \right\rangle \end{aligned} \tag{A10}$$

The sum of these two equations is $<(\Delta R')^2>$, giving

$$\left\langle (\Delta R')^2 \right\rangle = \left\langle (\Delta R)^2 \right\rangle + \left\langle (\Delta \beta)^2 \right\rangle \quad \text{(A11)}$$

Therefore, to calculate a particular granule's corrected $<(\Delta R)^2>$, we subtract the average radial motion $<(\Delta\beta)^2>$ measured on a bead of similar size and intensity from $<(\Delta R')^2>$ measured on a granule.

Statistical Accuracy of Corrected $<(\Delta z)^2>$

After correction for instrumental noise as above, the now-unbiased estimates for $<(\Delta z)^2>$ versus z (or intensity) still contain an uncertainty which arises from the random nature of z compounded by random instrumental noise. We estimate this uncertainty by a simulation program with random number generation.

The first step is to simulate the instrumental noise in intensity as a combination of photon count-independent CCD camera readout noise and photon count-dependent shot noise. The parameters describing this combination are phenomenologically set to produce photon count histograms that agree with the series of histograms observed experimentally on debris/bead samples.

Next, actual "granule" motions are simulated by generating a series of Δz values where the z motion steps are assumed to be Gaussian-distributed variables with variances corresponding to the corrected values found in the experiments at each particular mean intensity (or z) range. These simulated positions are converted to intensity, at which point simulated readout and shot noise are folded in according to the phenomenological parameters determined as described in the paragraph above and then converted back to $\Delta z'$, the set of which is now even noisier than the original Δz. The number of motions simulated at each mean intensity is set to be the same as the number that were actually accumulated at that intensity range in the experiments on chromaffin cell granules. With this set of simulated $\Delta z'$ values, the corresponding simulated $<(\Delta z')^2>$ could be calculated. Then the simulation is repeated again and again, each time giving new $<(\Delta z')^2>$ values (because the average is over a finite number of random values). The variance of this set, var $<(\Delta z')^2>$, could then be evaluated. The square root of this variance is the standard error (SE) in $<(\Delta z)^2>$. Twice that SE represents the 95% confidence range shown in Figure 1.

An alternative method that does not use simulation is based entirely on the variability in set of experimental $\Delta z'$ values at each intensity, using the definition of variance of the mean:

$$\mathrm{var}\left\langle (\Delta z')^2 \right\rangle = \frac{\left\langle \left[(\Delta z')^2 - \left\langle (\Delta z')^2 \right\rangle \right]^2 \right\rangle}{n-1} \quad \text{(A12)}$$

where n is the number of experimental $\Delta z'$ values that fall into a particular range of intensities. This method is only useful if there are enough such values in the intensity range to produce reliable statistics.

Statistical Accuracy of Corrected $<(\Delta R)^2>$

Actual granule motion steps in the x and y directions are each simulated as a Gaussian distributed variable with a variance corresponding to the corrected values found in the experiments at each particular intensity (or z) range. To this is added a random Gaussian-distributed step with a variance corresponding to the apparent "motion" of an immobile experimental bead arising from instrumental noise. From this sum, a $\Delta R'$ step is generated. The number of $\Delta R'$ motions simulated at each mean intensity is set to be the same as the number that were actually accumulated at that intensity range in the experiments on chromaffin cell granules. From this point on, the protocol for estimating the SE of the simulated values for $<(\Delta R)^2>$ is analogous to that for $<(\Delta z)^2>$ described above. The alternative method, based on actual variability in the set of experimental $\Delta R'$ values and an analogy to Eq. A12, can also be used.

Shot Noise Artifact in the Estimation of Sequential Motions

To determine whether the motion of a granule is *directed* rather than completely random, the interframe granule motion measured between two successive frames at times t and $t + 1$ ideally should be correlated with the immediately successive interframe motion measured between frames $t + 1$ and $t + 2$. In principle, a positive correlation shows that the motion persists in the same direction; a negative correlation shows that the motion tends to reverse itself; and a zero correlation indicates a random walk. In practice, however, a complication arises due to shot noise, which adds a randomness to the position measurement at any particular time, even if the granule is not moving at all. This complication gives rise to an apparent negative correlation in inferred granule motion between successive interframe intervals, even where one does not really exist. This effect occurs for both Δz and ΔR motions; the discussion here will refer to Δz for concreteness but it could be replaced by ΔR throughout.

First, assume shot noise is the only source of fluctuations in z. Given a shot noise generated "up-fluctuation" in the estimation for z at time $t + 1$, the measured Δz_1 [$\equiv z(t + 1) - z(t)$] in the $(t, t + 1)$ interval will tend to be *positive* because the immediately prior $z(t)$ measurement is equally likely to be an "up" or a "down" fluctuation. The immediately subsequent measured Δz_2 [$\equiv z(t + 2) - z(t + 1)$] then will tend to be *negative* because $z(t + 2)$ is equally likely to be an "up" or a "down" fluctuation. An analogous argument applies given a shot noise generated "down-fluctuation" in $z(t + 1)$, with the "positive" and "negative" words reversed. Therefore, Δz_1 and Δz_2 are negatively correlated. Qualitatively, the negative correlation arises because calculation of Δz_1 and Δz_2 both share the same input measurement $z(t + 1)$, one with a plus sign and the other with a minus sign. This artifact does *not* occur in comparing Δz_3 [$\equiv z(t + 3) - z(t + 2)$] with Δz_1, nor in comparing Δz_4 [$\equiv z(t + 4) - z(t + 3)$] with Δz_2.

The same conclusions apply even if the shot noise is mixed with actual motions in z. We assume that the measured $\Delta z'$ is composed of two independent parts: an actual z motion Δz and a shot noise contribution Δs:

$$\Delta z' = \Delta z + \Delta s \quad \text{(A13)}$$

The temporal autocorrelation function $G_{\Delta z'}$ for $\Delta z'$ is

$$\begin{aligned} G_{\Delta z'}(\tau) &= \langle \Delta z'(t + \tau)\Delta z'(t) \rangle \\ &= \langle [\Delta z(t + \tau) + \Delta s(t + \tau)][\Delta z(t) + \Delta s(t)] \rangle \\ &= G_{\Delta z}(\tau) + G_{\Delta s}(\tau) \end{aligned} \quad \text{(A14)}$$

The cross-terms in Eq A14 are zero because the actual motions and shot noise are uncorrelated. Variable s is the deviation from the actual z at any particular frame due to shot

noise, and can be positive or negative. The autocorrelation of the interframe shot noise is

$$\begin{aligned} G_{\Delta s} &= \langle \Delta s(t+\tau)\Delta s(t)\rangle \\ &= \langle [s(t+\tau+1) - s(t+\tau)][s(t+1) - s(t)]\rangle \\ &= \langle s(t+\tau+1)s(t+1) - s(t+\tau)s(t+1) - s(t+\tau+1)s(t) \\ &\quad + s(t+\tau)s(t)\rangle \\ &= G_s(\tau) - G(\tau-1) - G_s(\tau+1) + G_s(\tau) \\ &= 2G_s(\tau) - G_s(\tau-1) - G_s(\tau+1) \end{aligned} \tag{A15}$$

$G_s(\tau)$ has the well-known form of a positive delta function spike at $\tau = 0$; shot noise exhibits no correlation with itself from one instant to the next. The second term and the third term in Eq. A15 produce negative spikes at $\tau = 1$ and $\tau = -1$, respectively. It is these terms that represent the artifactual negative correlation at $\tau = \pm 1$ in $G_{\Delta z'}(\tau)$ in Eq. A14. There is no artifact at any other nonzero τ value.

Johns *et al*. (2001) show $G_{\Delta z'}(\tau)$ curves for z motion of secretory granules that display the negative correlation spike at $\tau = 1$. These were misinterpreted as being representative of actual z motions, but they are in fact shot noise artifacts. However, whether the artifact actually occurs depends on whether shot noise in intensity measurements is significant compared with the "noise" in intensity measurements generated by actual z motions. In the case of very bright objects, where the relative size of shot noise is small, the negative artifact at $\tau = 1$ may not be noticeable. In principle, the problem can be surmounted by calculating an autocorrelation of a modified $\Delta_k z'$ ($[\equiv z'(t+k) - z(t)]$ so that the negative spike artifact occurs at $\tau = \pm k$, where k represents a jump of many frames rather than just a single frame. If k is large enough, the artifact could be positioned beyond the temporal zone where actual z motions are correlated, thereby its contribution could be quantified.